

High-resolution x-ray spectra from molybdenum ions in the Alcator-C tokamak

E. Källne and J. Källne

Harvard-Smithsonian Astrophysical Observatory, Cambridge, Massachusetts 02138

Robert D. Cowan

Los Alamos National Laboratory, Los Alamos, New Mexico 87545

(Received 1 December 1982)

We report on measurements of the x-ray line emission in the wavelength region $\lambda=4.3-5.3$ Å from molybdenum in charge states between $28+$ and $32+$. The experimental results were compared with calculated line spectra (also presented) which facilitated the identification of many of the principal $2p-3d$, $2s-3p$, and $2p-3s$ transitions. Some indications of weaker satellite-line contributions were also found. The principal $2p-3d$ transitions were found to be the dominant ones. In particular, Mo^{32+} gave stronger contributions than other charge states for our plasma condition of $T_e=1.0-1.5$ keV while available calculations of relative ion abundances have predicted Mo^{32+} to be relatively strongest at $T_e=2.5-3.0$ keV.

I. INTRODUCTION

Characteristic x-ray emission from highly ionized impurity atoms in hot plasmas is a source of information on the ionization stages present in the plasma and is a means to diagnose the plasma conditions. The emission from high- Z elements, for instance, can reveal the relative importance of competing ionization-recombination processes which otherwise is difficult to observe for low- Z elements due to a strong Z dependence in the dielectronic-recombination rates.¹ Impurity ions from the walls and limiters of the vacuum vessel, while being transported into the plasma core, undergo successively increasing ionization mainly through electron-impact collisions. High- Z impurities, such as molybdenum, with $Z=42$, will be only partly stripped of their electrons at electron temperatures (T_e) of a few keV, common in tokamaks, in contrast to the more fully stripped low- Z elements. The high- Z elements have a large total excitation cross section, and the subsequent radiative deexcitations can cause large energy losses and eventually lead to major disruptions of the plasma. The stability and energy confinement of the plasma is therefore highly sensitive to the amount of high- Z impurities and the atomic properties of the species present.² In order to estimate the overall energy losses due to impurity radiation, modeling of the plasma radiative processes has been done using the best available atomic cross sections.^{2,3} However, the relative importance of the different ionization and excitation processes to the ionization stage buildup is not well known. Further-

more, the general assumption of a plasma in coronal equilibrium has not been verified by experiments for tokamak plasmas, nor has the assumption that heavy impurities will be in ionization equilibrium.^{4,5} Therefore it is of utmost importance to identify the emission spectra responsible for heavy radiation losses in the plasma.

The spectra of heavy, partially stripped ions of high- Z elements such as molybdenum at temperatures of a few keV are composed of lines from many multicharge states, each having a complex level structure. The line spectrum of each ion can be calculated with some confidence only if there is available supporting experimental information. This has been demonstrated in some recent spectroscopic investigations of high- Z elements in plasmas.⁶⁻⁸ The relative complexity of the spectra requires, first of all, experiments with high-energy resolution in order to separate and identify individual emission lines. Even so, all cases are still not amenable to spectral investigations since the measured spectrum consists of simultaneous emission from several successive ionization stages which produces quasicontinuous features superimposed on the continuum (bremsstrahlung) emission background.⁹ However, for ions characterized by closed-shell atomic configurations, the emission spectra are experimentally resolvable allowing line identification with the help of calculated spectra. For these cases, important conclusions can be reached concerning the major ionization and excitation processes of these ions embedded in the hot plasma usually consisting of hydrogen or deuterium. In this paper we report on measurements of

the x-ray line emission from molybdenum impurities in the plasma of the Alcator-C tokamak¹⁰ in the wavelength region 4.3–5.3 Å, which covers strong $n = 2$ and 3 transitions from molybdenum in neon-like and adjacent charge states.

II. EXPERIMENTAL

The experiment was performed at the high-field, high-density tokamak Alcator-C located at MIT.¹⁰ The magnetically confined plasma is physically limited by two molybdenum rings (radius 16 cm) inside the vacuum vessel. An x-ray spectrometer views the plasma along a central chord at one of the limiter ports with an instrumental vertical aperture corresponding to ~ 5 cm of the central part of the plasma. The incident photon flux is defined by an entrance slit (0.2-mm wide) which is located about 60 cm from the plasma center. A beryllium window of thickness 0.04 mm at the slit separates the vacuum of the tokamak and the spectrometer. The spectral analysis is done with a cylindrically curved ($R = 58.5$ cm) Bragg diffracting crystal [pentaerythritol (PET) $2d_{002} = 8.742$ Å] which disperses the photons along the direction parallel to the horizontal cylinder axis. The photons are counted with a position-sensitive detector consisting of a 10-cm single wire proportional counter and standard electronics. A multichannel analyzer stores and displays the spectrum before the data are transferred to the common data acquisition system at the tokamak using a Digital Equipment Corporation PDP 11/30 computer. In this way an extended spectrum can be recorded simultaneously for individual plasma discharges and partially analyzed between shots. The useful bandwidth of each such spectrum is about 0.4 Å and the full wavelength region $\lambda = 4.3$ –5.3 Å of the spectrometer was covered by appropriately positioning the detector. Other details about the experimental setup have been discussed in earlier papers.^{11,12}

The x-ray emission in the 4.3–5.3-Å region can be studied under varying conditions of the main plasma parameters. The molybdenum line emission, however, is measurable only under rather limited plasma conditions because the molybdenum we observed is an ambient impurity in the plasma of hydrogen or deuterium. The impurity concentration is therefore controllable but found to be high only for low densities and seems to rise sharply with decreasing electron density N_e (or increasing T_e , since T_e and N_e are inversely correlated in Alcator-C). The impurity level of molybdenum ions seems to have a different plasma dependence than has that of low- Z impurities, such as sulfur (see Fig. 1). Thus the Mo line spectra measured here represent a rather narrow

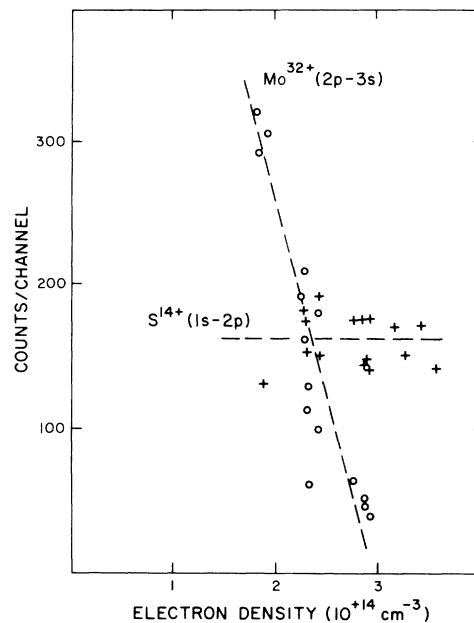


FIG. 1. Emission intensity variations from S^{14+} ($1s-2p$) and Mo^{32+} ($2p-3s$) for different electron densities \bar{N}_e .

band of plasma parameters, namely, electron densities of $N_e = (1.5-3) \times 10^{14} \text{ cm}^{-3}$ (as determined from laser interferometer measurements) and electron temperatures of $T_e \approx 1.0$ –1.5 keV (as determined from the x-ray continuum measurements).

The plasma conditions as characterized by parameters such as plasma current, electron density, and electron temperature are essentially constant over a period of some 100–200 msec in the middle of the discharge. Our measurements were electronically gated to pick out the emission during the constant part of the discharge. Hence the time scale of observation was long compared to typical ionization-recombination times.

An example of the time history for a typical plasma discharge is shown in Fig. 2. Here we can compare the time dependence of plasma current and electron density with the signal from the integrated ($h\nu > 1$ keV) x-ray emission and our x-ray signal. Our signal for this discharge represents largely the time dependence of the Mo line emission over the wavelength region 4.5–4.9 Å.

The time dependence of the x-ray emission over the wavelength band of the detector ($\Delta\lambda = 0.4$ Å) was recorded for each discharge with a time resolution of typically 1 msec. As exemplified in Fig. 2, the temporal dependence of the molybdenum emission was generally found to follow that of the plas-

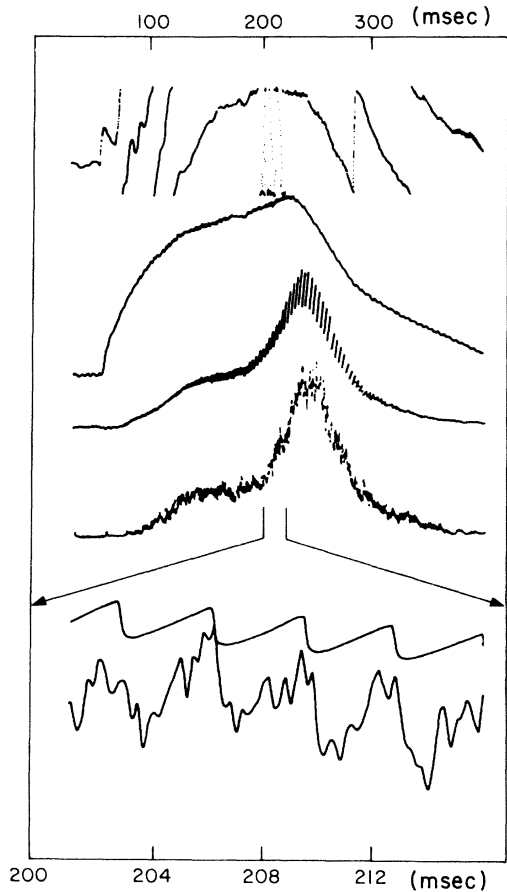


FIG. 2. Time evolution of a typical plasma shot. Traces from the top to the bottom show plasma density \bar{N}_e 0.58×10^{14} cm $^{-3}$ /fringe, plasma current (I_p) 400 kA at peak, soft x-ray emission ($h\nu > 1$ keV), high-resolution x ray. Lowest two traces are 25-fold temporal expansions of the third and fourth traces to show the sawtooth instability.

ma current. However, at the time in the middle of the discharge ($T \sim 180$ msec) where ohmic heating is applied, the Mo emission shows a strong rise compared to relative moderate rise in current. An interesting observation can be made in the comparison of the Mo line emission and the total (broadband) x-ray emission, both measured along the central plasma chord. The total emission is commonly used, for instance, to detect the characteristic $m = 1$ plasma instabilities. Another temporal feature of the plasma discharge is the so-called sawtooth instability with a time period of some 4 msec. The presence of this instability is generally detected in the broadband x-ray emission, and here we demonstrate that this can be seen also in the molybdenum line emission (Fig. 2). Moreover, since the sawtooth in-

stabilities are believed to belong to the core region of the plasma inside the $m = 1$ surface, this portion of our line of sight (limited vertically to the central 5 cm of the plasma) is an important contributor to the measured emission from the radial impurity ion profiles. While the sawtooth instabilities are seen in our signal from the highly ionized molybdenum, they are not as apparent in the emission from heliumlike ions (such as chlorine or sulfur), which is consistent with the expectedly broader spatial profiles of these ions. Yet, the time-resolved emission from the hydrogenlike sulfur (having a higher ionization potential) again shows a time behavior with sawtooth instabilities; the x-ray emission from S and Cl has been discussed earlier.^{11,13,14}

III. THEORETICAL CALCULATIONS

Previous experimental work on the x-ray line emission in molybdenum has led to the identification of Mo XXXIII lines at 4.415, 4.630, 4.804, 4.982, and 5.207 Å.^{15,16} These identifications are reasonably firm and can be used in support of the interpretation of other lines in Mo spectra with the aid of theoretical calculations employing the Slater-Condon theory of atomic structure.¹⁷ One-electron radial wave functions were computed via the Hartree-Fock radial functions (HFR) method,¹⁸ which uses Hartree-Fock equations with inclusion of mass-velocity and Darwin terms that provide first-order corrections for (spin-independent) relativistic effects. The Hamiltonian matrices were evaluated using these radial functions and diagonalized to give eigenvalues (energy levels) and eigenvectors (N -electron intermediate-coupling wave functions) in the usual way. For this purpose, all Coulomb radial integrals F^k , G^k , and R^k (contributing to matrix elements through terms other than the configuration center-of-gravity energy E_{av}) were scaled down by a factor of 0.93 to allow for weak configuration-interaction effects and thereby improve agreement between computed and observed wavelengths; the Blume-Watson spin-orbit radial integrals ξ were similarly scaled by a factor of 0.98.

Configuration interactions of the type $3s3d + 3p^2$ are important because of the near equality in energy of the corresponding configurations and were included where pertinent, as in calculation of the transition arrays

$$\text{Mo XXXII } 2p^6 3s - (2p^5 3s 3d + 2p^5 3p^2)$$

and

$$\text{Mo XXXI } 2p^6 3s^2 - (2p^5 3s^2 3d + 2p^5 3s 3p^2).$$

Trial calculations showed other configuration interactions to be unimportant, and most of these were

TABLE I. Calculated wavelengths and gf values for Mo 2s-3p and 2p-3s transitions.

	λ (Å)	gf	Classification	
Mo 2s-3p	4.412	0.46	Mo ³²⁺ 2s ² 2p ⁶ 1S ₀ -(2s _{1/2} 2p ⁶ 3p _{3/2}) ₁	
	4.458	0.17	Mo ³²⁺ 2s ² 2p ⁶ 1S ₀ -(2s _{1/2} 2p ⁶ 3p _{1/2}) ₁	
	4.425	0.18	Mo ³¹⁺ 2s ² 2p ⁶ 3s ² 2S _{1/2} -(2s _{1/2} , 3s 3p ¹ P ₁) _{1/2}	
	4.450	0.68	Mo ³¹⁺ 2s ² 2p ⁶ 3s ² 2S _{1/2} -(2s _{1/2} , 3s 3p ³ P ₂) _{3/2}	
	4.479	0.21	Mo ³¹⁺ 2s ² 2p ⁶ 3s ² 2S _{1/2} -(2s _{1/2} , 3s 3p ³ P ₁) _{1/2}	
	4.500	0.12	Mo ³¹⁺ 2s ² 2p ⁶ 3s ² 2S _{1/2} -(2s _{1/2} , 3s 3p ³ P ₁) _{3/2}	
	4.477	0.44	Mo ³⁰⁺ 2s ² 2p ⁶ 3s ² 1S ₀ -(2s _{1/2} , 3p _{3/2}) ₁	
	4.523	0.16	Mo ³⁰⁺ 2s ² 2p ⁶ 3s ² 1S ₀ -(2s _{1/2} , 3p _{1/2}) ₁	
	4.482		Mo ³⁰⁺ 2s ² 2p ⁶ 3s ² 1S ₀ -(2s _{1/2} , 3p _{3/2}) ₂ (M2)	
	Mo 2p-3s	4.980	0.09	Mo ³²⁺ 2p ⁶ 1S ₀ -(2p ⁵ _{1/2} 3s _{1/2}) ₁
		5.204	0.12	Mo ³²⁺ 2p ⁶ 1S ₀ -(2p ⁵ _{3/2} 3s _{1/2}) ₁
		5.212		Mo ³²⁺ 2p ⁶ 1S ₀ -(2p ⁵ _{3/2} 3s _{1/2}) ₂ (M2)
5.024		0.048	Mo ³¹⁺ 2p ⁶ 3s ² 2S _{1/2} -(2p ⁵ _{1/2} 3s ²) _{1/2}	
5.256		0.091	Mo ³¹⁺ 2p ⁶ 3s ² 2S _{1/2} -(2p ⁵ _{3/2} 3s ²) _{3/2}	
5.064		0.060	Mo ³⁰⁺ 2p ⁶ 3s 3p ³ P ₂ -(2p ⁵ _{1/2} 3s ² 3p _{3/2}) ₂	
5.067		0.057	Mo ³⁰⁺ 2p ⁶ 3s 3p ³ P ₂ -(2p ⁵ _{1/2} 3s ² 3p _{3/2}) ₁	
5.069		0.024	Mo ³⁰⁺ 2p ⁶ 3s 3p ³ P ₀ -(2p ⁵ _{1/2} 3s ² 3p _{1/2}) ₁	
5.079		0.042	Mo ³⁰⁺ 2p ⁶ 3s 3p ³ P ₁ -(2p ⁵ _{1/2} 3s ² 3p _{1/2}) ₁	
5.111		0.054	Mo ³⁰⁺ 2p ⁶ 3s 3p ³ P ₁ -(2p ⁵ _{3/2} 3s ² 3p _{3/2}) ₂	
5.305		0.16	Mo ³⁰⁺ 2p ⁶ 3s 3p ³ P ₂ -(2p ⁵ _{3/2} 3s ² 3p _{3/2}) ₃	
5.311		0.044	Mo ³⁰⁺ 2p ⁶ 3s 3p ³ P ₀ -(2p ⁵ _{3/2} 3s ² 3p _{1/2}) ₁	
	0.103	Mo ³⁰⁺ 2p ⁶ 3s 3p ³ P ₁ -(2p ⁵ _{3/2} 3s ² 3p _{1/2}) ₂		

neglected.

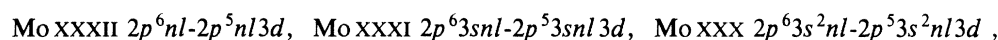
The principal lines computed for 2s-3p, 2p-3s, and 2p-3d excitations in Ne-like to Mg-like molybdenum are listed in Tables I and II. Level designations are given in the J_1 - J_2 coupling representation for two-open-subshell configurations and in the

$$[J_1, (L_{23}S_{23})J_{23}]_J$$

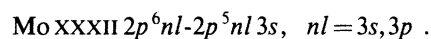
representation for three-open-subshell cases. Although these representations are the best possible

ones to use, basis-state mixings are usually large (especially where 3s3d + 3p² configuration mixings are present), and level designations must consequently not always be taken literally.

Calculations were also made for analogous transitions of collisionally excited states in Al-like and Si-like molybdenum and for the following satellite-line transition arrays produced as the result of dielectronic recombination:



$$nl = 3s, 3p, 3d, 4s, 4p, 4d, 4f$$



The results are too complex and voluminous to present here and are in any case of relatively little importance in interpretation of the strong observed lines.

The above results for Ne-like through Si-like molybdenum have been used to synthesize spectra, using simple methods of computing excitation and

dielectronic-recombination rates to obtain intensities of the various lines, and including Doppler and instrumental line broadening. Some details have been discussed elsewhere.¹⁹ The results of these calculations are presented in Tables III–V (see also Figs. 4–8) for comparison with the experimental results. Computed wavelengths are accurate to about

TABLE II. Calculated wavelengths and gf values for Mo 2p-3d transitions.

	λ	gf	Classification
Mo 2p-3d	4.627	1.71	Mo ³²⁺ 2p ⁶ 1S ₀ -(2p ⁵ _{1/2} 3d _{3/2}) ₁
	4.802	1.84	Mo ³²⁺ 2p ⁶ 1S ₀ -(2p ⁵ _{3/2} 3d _{5/2}) ₁
	4.855	0.001	Mo ³²⁺ 2p ⁶ 1S ₀ -(2p ⁵ _{3/2} 3d _{3/2}) ₁
	4.628	0.74	Mo ³¹⁺ 2p ⁶ 3s ² S _{1/2} -0.65(2p ⁵ _{1/2} 3s 3d ¹ D ₂) _{3/2} +0.31(2p ⁵ _{1/2} 3p ² 1D ₂) _{3/2}
	4.659	1.15	Mo ³¹⁺ 2p ⁶ 3s ² S _{1/2} -0.98(2p ⁵ _{1/2} 3s 3d ³ D ₁) _{1/2}
	4.665	1.36	Mo ³¹⁺ 2p ⁶ 3s ² S _{1/2} -0.86(2p ⁵ _{1/2} 3s 3d ³ D ₂) _{3/2}
	4.693	0.09	Mo ³¹⁺ 2p ⁶ 3s ² S _{1/2} -0.28(2p ⁵ _{1/2} 3s 3d ³ D ₁ , 1D ₂) _{3/2} +0.69(2p ⁵ _{1/2} , 3p ² 1D ₂ , 3P ₁) _{3/2}
	4.813	0.78	Mo ³¹⁺ 2p ⁶ 3s ² S _{1/2} -0.48(2p ⁵ _{3/2} 3s 3d ¹ D ₂ , 3D ₃) _{3/2} +0.49(2p ⁵ _{3/2} , 3p ² 1D ₂ , 3P ₂) _{3/2}
	4.819	0.81	Mo ³¹⁺ 2p ⁶ 3s ² S _{1/2} -0.74(2p ⁵ _{3/2} 3s 3d ¹ D ₂ , 3D ₂) _{1/2} +0.20(2p ⁵ _{3/2} , 3p ² 1D ₂) _{1/2}
	4.834	0.46	Mo ³¹⁺ 2p ⁶ 3s ² S _{1/2} -0.20(2p ⁵ _{3/2} 3s 3d ³ D ₃ , 1D ₂) _{3/2} +0.76(2p ⁵ _{3/2} , 3p ² 1S ₀ , 3P ₀ , 3P ₂) _{3/2}
	4.842	1.18	Mo ³¹⁺ 2p ⁶ 3s ² S _{1/2} -0.52(2p ⁵ _{3/2} 3s 3d ³ D ₃) _{3/2} +0.44(2p ⁵ _{3/2} , 3p ² 1S ₀ , 3P ₂ , 1D ₂ , 3P ₀) _{3/2}
	4.860	0.36	Mo ³¹⁺ 2p ⁶ 3s ² S _{1/2} -0.66(2p ⁵ _{3/2} 3s 3d ³ D ₂ , 3D ₁) _{1/2} +0.29(2p ⁵ _{3/2} , 3p ² 1D ₂ , 3P ₁) _{1/2}
	4.674	1.30	Mo ³⁰⁺ 2p ⁶ 3s ² 1S ₀ -0.77(2p ⁵ _{1/2} 3s ² 3d _{3/2}) ₁ +0.16(2p ⁵ _{1/2} , 3s 3p ² 2D _{3/2}) ₁
	4.688	0.05	Mo ³⁰⁺ 2p ⁶ 3s ² 1S ₀ -0.77(2p ⁵ _{1/2} 3s ² 3d _{3/2}) ₁ +0.74(2p ⁵ _{1/2} , 3s 3p ² 2P _{3/2}) ₁
	4.696	0.06	Mo ³⁰⁺ 2p ⁶ 3s ² 1S ₀ -0.77(2p ⁵ _{1/2} 3s ² 3d _{3/2}) ₁ +0.91(2p ⁵ _{1/2} , 3s 3p ² 2S _{1/2} , 2P _{1/2} , 2P _{3/2}) ₁
	4.726	0.13	Mo ³⁰⁺ 2p ⁶ 3s ² 1S ₀ -0.77(2p ⁵ _{1/2} 3s ² 3d _{3/2}) ₁ +0.80(2p ⁵ _{1/2} , 3s 3p ² 2P _{1/2} , 2D _{3/2} , 2S _{1/2}) ₁
	4.752	0.13	Mo ³⁰⁺ 2p ⁶ 3s ² 1S ₀ -0.77(2p ⁵ _{1/2} 3s ² 3d _{3/2}) ₁ +0.79(2p ⁵ _{1/2} , 3s 3p ² 2D _{3/2} , 2P _{1/2}) ₁
	4.850	0.95	Mo ³⁰⁺ 2p ⁶ 3s ² 1S ₀ -0.50(2p ⁵ _{3/2} 3s ² 3d _{5/2,3/2}) ₁ +0.27(2p ⁵ _{3/2} , 3s 3p ² 2P _{3/2}) ₁
	4.866	0.74	Mo ³⁰⁺ 2p ⁶ 3s ² 1S ₀ -0.40(2p ⁵ _{3/2} 3s ² 3d _{5/2}) ₁ +0.45(2p ⁵ _{3/2} , 3s 3p ² 2P _{3/2}) ₁
	4.939	0.09	Mo ³⁰⁺ 2p ⁶ 3s ² 1S ₀ -0.40(2p ⁵ _{3/2} 3s ² 3d _{5/2}) ₁ +0.79(2p ⁵ _{3/2} , 3s 3p ² 4P _{5/2} , 2D _{5/2}) ₁

$\pm 0.1\%$, so that identification of observed lines can be considered fairly firm provided computed and observed wavelengths agree to within ± 0.005 Å. While it is necessary to compare computed and observed intensities in order to corroborate identifica-

tions based on wavelength, quantitative agreement cannot be expected because of the rough collisional excitation rates employed,²⁰ neglect of cascades and autoionization effects, possible nonequilibrium effects, etc.

TABLE III. Comparison of experimental wavelengths and intensities in the λ region 4.4–4.6 Å with predicted Mo 2s-3p transitions from Mo²⁹⁺–Mo³²⁺. Distinction is made between states excited by electron collisions and dielectronic recombination.

Figure keys	λ_{expt} (Å)	$I_{\text{expt}}^{\text{rel}}$	Figure keys	λ_{theor} (Å)	$I_{\text{theor}}^{\text{rel}}$	Ionization stages		
						Resonance transition	$I \left[\frac{\text{dielectronic}}{\text{collision}} \right]$	
a	4.418	100	1	4.412	100	32 +		
	b	4.424	47	2	4.426	28	31 +	
		4.444 ^a		3	4.450	110	Cl ¹⁵⁺ (1s ² 1S ₀ -1s 2p ¹ P ₁)	
	4.464		4	4.458	37	31 +		
		4.468				32 +	Cl ¹⁵⁺ (1s ² 1S ₀ -1s 2p ³ P _{2,1})	
c	4.497 ^a		5	4.478	135	30 +		
	4.503	53	6	4.500	20	Cl ¹⁵⁺ (1s ² 1S ₀ -1s 2s ³ S ₁)		
			7	4.510	35	31 +		
			8	4.523	41	29 +		
						30 +		

^aCalibration lines from Refs. 21 and 22.

TABLE IV. Comparison of experimental wavelengths and intensities in the λ region 4.6–4.9 Å with Mo $2p$ - $3d$ transitions from Mo²⁸⁺ – Mo³²⁺.

Figure keys	λ_{expt} (Å)	$I_{\text{expt}}^{\text{rel}}$	Figure keys	λ_{theor} (Å)	$I_{\text{theor}}^{\text{rel}}$	Resonance transition	Ionization stages	
							I	$\left[\frac{\text{dielectronic collision}}{\text{collision}} \right]$
<i>a</i>	4.630	47	1	4.626	104	32 +		
<i>b</i>	4.635	18	2	4.628	28	31 +		
			3	4.643	7			31 + (3 <i>p</i>)
<i>c</i>	4.648	8	4	4.648	7			31 + (3 <i>p</i>)
<i>d</i>	4.664	38	5	4.659	71	31 +		31 + (3 <i>d</i>) + 30 + (3 <i>p</i>)
<i>e</i>	4.668	37	6	4.665	54	31 +		30 + (3 <i>d</i>)
<i>f</i>	4.680	82	7	4.674 + 4.675	100	30 +		30 + (3 <i>p</i> + 3 <i>d</i>)
			8	4.689	28	31 + , 30 + , 29 +		31 + (3 <i>p</i> + 3 <i>d</i>), 30 + (3 <i>p</i>)
			9	4.693	23	29 +		30 + (3 <i>p</i> + 3 <i>d</i>)
			10	4.699	23	29 +		30 + (3 <i>p</i> + 3 <i>d</i>)
			11	4.705	21	29 +		30 + (3 <i>p</i>)
			12	4.708	21	29 +		30 + (3 <i>p</i>)
<i>g</i>	4.716	16	13	4.723	22	30 + + 29 +		30 + (3 <i>d</i> + 3 <i>p</i>)
			14	4.726	22	S^{15+} (1 <i>s</i> ² <i>S</i> _{1/2} -2 <i>p</i> ² <i>P</i> _{3/2})		
<i>h</i>	4.804 ^a	100	15	4.740-4.751	12	S^{15+} (1 <i>s</i> ² <i>S</i> _{1/2} -2 <i>p</i> ² <i>P</i> _{1/2})		
<i>i</i>	4.808	22	16	4.802	100	29 + + 30 +		
<i>j</i>	4.816	17	17	4.813	29	31 +		
<i>k</i>	4.825	24	18	4.820	30	31 +		
<i>l</i>	4.837	22	19	4.833	46	31 +		
<i>m</i>	4.846	47	20	4.842	67	31 +		31 + (3 <i>p</i>)
<i>n</i>	4.854	30	21	4.850	83	30 +		31 + (3 <i>d</i> + 3 <i>p</i>), 30 + (3 <i>p</i>)
			22	4.855	32 +	32 +		31 + (3 <i>d</i> + 3 <i>p</i>), 30 + (all)
			23	4.858	29	31 +		30 + (3 <i>p</i> + 3 <i>d</i>)
<i>o</i>	4.869	24	24	4.866	83	30 +		30 + (3 <i>p</i> + 3 <i>d</i>)
<i>p</i>	4.888	11	25	4.800–4.883	16	29 +		30 + (3 <i>d</i> + 3 <i>p</i>)
			26	4.887	12	29 +		
<i>q</i>	4.896	17	27	4.899	17	29 +		30 + (3 <i>d</i>)
<i>r</i>	4.906	18	28	4.905	10	29 +		30 + (3 <i>p</i> + 3 <i>d</i>)
			29	4.931	9	28 + + . . .		
			30	4.940	8	30 + , 29 + , 28 +		

^aCalibration wavelengths from Refs. 15 and 21.

TABLE V. Comparison of experimental wavelengths and intensities in the λ region 4.9–5.2 Å with Mo $2p$ - $3s$ transitions from Mo^{28+} – Mo^{32+} .

Figure keys	λ_{expt} (Å)	$I_{\text{expt}}^{\text{rel}}$	Figure keys	λ_{theor} (Å)	$I_{\text{theor}}^{\text{rel}}$	Resonance transition	Ionization stages	
							I	$\left[\frac{\text{dielectronic collision}}{\text{recombination}} \right]$
<i>a</i>	4.982	100	1	4.979	100			
<i>b</i>	5.012	19	2	5.003	9			
			3	5.008	70			1.0
<i>c</i>	5.038 ^a	267	4	5.024	31 +	$S^{14+}(1s^2 1S_0 - 1s 2p^1 P_1)$		
	5.049	53						
	5.062	40						
	5.063	80						
<i>d</i>	5.065		5	5.066	22	$S^{14+}(1s^2 1S_0 - 1s 2p^3 P_{2,1})$		
<i>e</i>	5.101 ^a							
	5.155	20						
<i>f</i>	5.163	13						
	5.207	35						
<i>g</i>	5.217	24	6	5.204	234			
	5.238	2	7	5.212	32 +	$S^{13+}(1s^2 2s - 1s 2s 2p^2 P)$		
<i>i</i>	5.259	6						
	5.274	5	8	5.256	130	$S^{14+}(1s^2 1S_0 - 1s 2s^3 S_1)$		
<i>k</i>	5.281	3						
			9	5.304	0.33	$32 + (\text{magnetic quadrupole}) 2p^6 1S_0 - 2p^5 3s^3 P_2$		
<i>l</i>								31 + (2p)

^aCalibration wavelengths from Refs. 21 and 22.

IV. RESULTS

Figure 3 shows an example of the x-ray emission observed from the Alcator-C plasma in the wavelength region 4.3–5.3 Å. In order to produce this spectrum, which represents the full (normal) bandwidth of the spectrometer, several similar plasma shots were used with three different detector settings. The plasma conditions were chosen so that the Mo emission was favored although some characteristic emission from sulfur and chlorine impurities is also visible. The spectra of heliumlike chlorine and sulfur, and of hydrogenlike sulfur along with their plasma diagnostics implications have been discussed elsewhere.^{11,14}

Here we shall concentrate on the spectrum of molybdenum. It is obvious from Fig. 3 that Mo impurities in the plasma produce numerous lines in the region 4.3–5.3 Å, the identification of which we shall organize by type of transition, i.e., $2s-3p$, $2p-3d$, and $2p-3s$. These correspond to predicted lines lying in the wavelength regions 4.3–4.5, 4.6–4.9, and 4.9–5.3 Å, respectively, as summarized in Tables III–V. The measured line spectra are shown in Figs. 4–8. Each of these spectra covers part of the wavelength region 4.3–5.3 Å so that the $2s-3p$ lines appear in Fig. 4, the $2p-3d$ lines in Figs. 4–6, and the $2p-3s$ lines in Figs. 6–8. Figure 8 shows the results where the spectrometer was adjusted to reach $2p-3s$ lines beyond $\lambda=5.3$ Å. Below, we discuss the results in more detail.

A. $2p-3d$ transitions

Figure 5 shows the experimental and calculated spectra in the region 4.6–4.9 Å, containing $2p-3d$ transitions in molybdenum. The experimental spectrum is from a single detector setting and was accumulated over 12 similar plasma discharges to provide better counting statistics. The plasma conditions were characterized by an electron density of $3 \times 10^{14} \text{ cm}^{-3}$ and an electron temperature of $T_e \sim 1400 \text{ eV}$. To fix the wavelength scale we used the H-like sulfur resonance transitions $1s-2p$ at $\lambda=4.726$ and 4.731 Å (Ref. 21) and the Mo^{32+} $2p-3d$ transition at 4.804 Å (Ref. 15); wavelengths used for calibration are marked with an a in Tables III–V. Each distinct peak in the measured spectrum has been assigned a letter and is similarly referred to in Table IV. The theoretical spectrum shows the relative line intensities as determined by the collisional excitation and dielectronic-recombination rates for a plasma temperature $T_e = 1.2 \text{ keV}$. It was assumed that the plasma was principally in coronal equilibrium, but the relative population densities of the different charge states as predicted by the coronal approximation has to be shifted to better match our experimental intensities (see below). The lines of the calculated spectrum are identified by numbers which also are used in Table IV. Table IV gives a summary of the experimental and theoretical results on wavelengths and relative intensities, and each line is identified as to ion

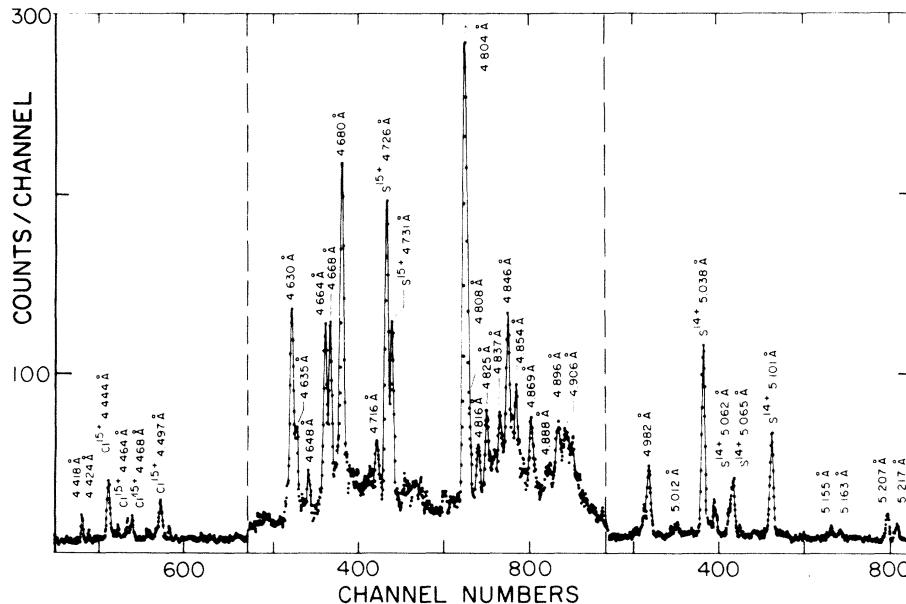


FIG. 3. Spectrum over the full wavelength range. Composed from three different detector settings. Wavelengths and identifications are indicated directly at the strong peaks. Plasma conditions for the spectrum were $\bar{N}_e = 2.5 \times 10^{14} \text{ cm}^{-3}$ and $T_e = 1.3 \text{ keV}$.

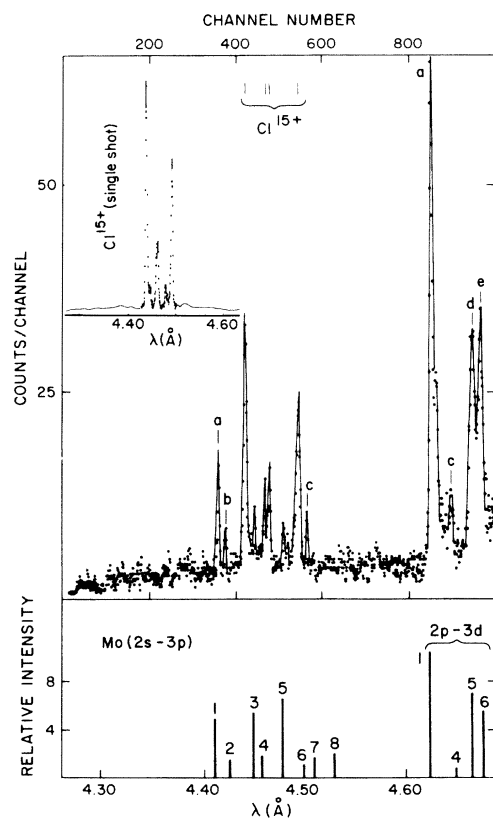


FIG. 4. Comparison of experimental and theoretical spectra in the region of Mo $2s-3p$ and $2p-3d$. Observed peaks are keyed with letters and the predicted ones with numbers referred to in Tables III ($2s-3p$) and IV ($2p-3d$). Experimental spectrum is an addition of two shots at plasma conditions of $\bar{N}_e = 1.7 \times 10^{14} \text{ cm}^{-3}$ and $T_e \approx 1.4 \text{ keV}$. Insert shows the spectrum from a single plasma shot with only emission from chlorine present.

charge state and as to whether it is a resonance or satellite transition.

From the comparison of experimental and theoretical results in Fig. 5, we see that most of the observed prominent features can be understood in terms of $2p-3d$ transitions. Of note is that the only strong lines that lack theoretical counterparts, i.e., the doublet at 4.73 Å, have previously been identified as the $1s_{1/2}-2p_{3/2,1/2}$ doublet of H-like sulfur. The wavelength agreement for the stronger lines is within about 5 mÅ, i.e., consistent with the expected theoretical accuracy of 0.1%. It may be noted that the predicted separation of the spin-orbit components seems to be systematically slightly too large for each charge state, so that the theoretical HFR spin-orbit radial integrals ξ_{2p} should have been scaled down by a factor of 0.97 rather than 0.98. For comparison, nonrelativistic HF values of ξ_{2p} are 7% smaller than HFR values. The experimental

data clearly provide a sensitive test of the theoretical assumptions. At a more detailed level of the line identification, we make the following observations.

Among the prominent lines of the Ne-like spectrum of Mo^{32+} are the $2p-3d$ transitions at 4.630 and 4.804 Å which are the predicted lines 1 and 16. These lines always appear in plasma shots showing any Mo emission at all. The third line in the $2p-3d$ array, predicted to be at 4.855 Å (line number 22 in Fig. 5), could contribute to the observed peak (n) although other charge states (Mo^{30+} and Mo^{31+}) might be even stronger contributors in this wavelength region (cf. Table IV). The presence of Mo^{32+} in the plasma, however, is in no doubt, and it is further corroborated by the observation of strong $2p-3s$ transitions as discussed below. Besides these three principal lines of the Ne-like Mo spectrum, the theory predicts contributions from dielectronic satellites (lines 3–7 in Fig. 5). These appear on the long-wavelength side of the 4.630 Å line and near the 4.804 Å line. In fact, the region $\lambda = 4.806\text{--}4.900 \text{ Å}$ contains a number of observed peaks ($i\text{--}m$, for instance) which each may contain one or several of these satellites. The potential satellite lines in this region are usually weaker than those in the short-wavelength part of the spectrum, which is in qualitative agreement with the calculations. However, besides these dielectronic satellites, there are many resonance transitions of lower charge states of molybdenum to consider as well.

The emission from Mo^{31+} produces a more complex spectrum since each $2p-3d$ transition seen in Mo^{32+} can be split into several components. Indeed, corresponding to the two strong lines seen in Mo^{32+} at 4.630 and 4.804 Å, we see for Mo^{31+} two sets of peaks (b, d, e) and (j, k, l, m) that match up well to the predicted lines (2, 5, 6) and (17, 18, 19, 20) (Fig. 5 and Table IV). These lines group together according to the $2p_{1/2}$ and $2p_{3/2}$ spin-orbit separation of the higher atomic state. Again, the calculated spin-orbit separation for this Na-like spectrum is systematically slightly greater than what is observed.

Finally, emission from Mo^{30+} is evidenced by the peaks at 4.680 Å (f) and at 4.854 Å (n) which we associate with predicted lines 7 and 21 of the Mg-like spectrum (Fig. 5 and Table IV). The latter identification, however, cannot be claimed with the same certainty due to the multitude of predicted lines and the rather vague experimental peak profiles in this region. It is interesting to note that the line f at 4.680 Å is always observed to be one of the dominant features in the spectrum of molybdenum emission, along with the two strong Mo^{32+} lines at 4.630 and 4.804 Å. Moreover, besides the three main ionization stages, Mo^{32+} , Mo^{31+} , and Mo^{30+} , we see contributions in the wavelength regions 4.685–4.800

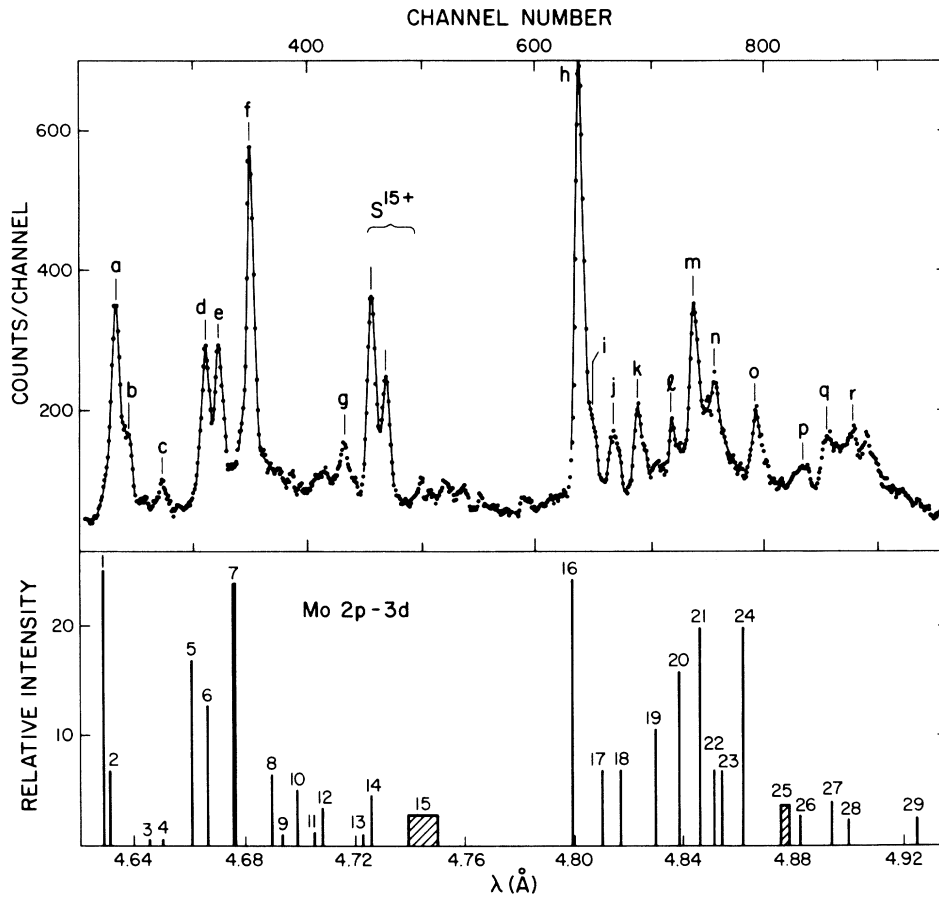


FIG. 5. Comparison of experimental and theoretical x-ray spectra in the region of Mo $2p$ - $3d$ emission. Peaks in the experimental spectrum have been keyed with letters and the calculated peaks with numbers referred to in Table IV. Experimental wavelength scale has been normalized to the peak (h) at 4.804 Å. Experimental spectrum is an addition of 12 shots at $\bar{N}_e = 3.0 \times 10^{14} \text{ cm}^{-3}$ and $T_e \approx 1.4 \text{ keV}$.

Å and 4.880–4.950 Å which could be attributed to emission from lower ionization stages as indicated in Table IV. However, these Mo $^{28+}$ and Mo $^{29+}$ contributions are mostly very weak compared to the generally dominant Mo $^{32+}$ lines.

We have thus been able to firmly identify the presence of Mo $^{32+}$, Mo $^{31+}$, and Mo $^{30+}$. The fact that Mo $^{32+}$ dominates the emission for our plasma conditions is surprising in view of current equilibrium calculations^{4,5} which predict that Mo $^{32+}$ should be the predominant charge state only at temperatures of $T_e = 2$ – 3 keV , i.e., considerably higher than the diagnosed temperature of 1–1.5 keV for the Alcator-C plasma. Our results therefore suggest that the ionization rates used in the calculated abundance ratios are too low for the higher ionization states, the recombination rates are too high, or that the charge states of the molybdenum ions are not distributed according to coronal equilibrium condi-

tions. In the atomic calculations presented in the present work we have corrected for this apparent discrepancy between observed and tabulated abundance ratios and adopted semiempirical abundance ratios to predict the relative intensities of the emission from different charge states: we used relative abundances of 0.08, 0.13, 0.20, 0.25, and 0.17 for Mo $^{28+}$ –Mo $^{32+}$, whereas the coronal equilibrium model at a temperature of 1.2 keV gives 0.18, 0.27, 0.13, 0.07, and 0.005, respectively.^{4,5} The relative intensities given in Table IV have been normalized arbitrarily to the line at 4.804 Å.

B. $2p$ - $3s$ transitions

Figure 7 shows the x-ray emission in the wavelength region of 4.9–5.2 Å where we expect major contributions from $2p$ - $3s$ transitions of molybdenum. This region also contains the well-known

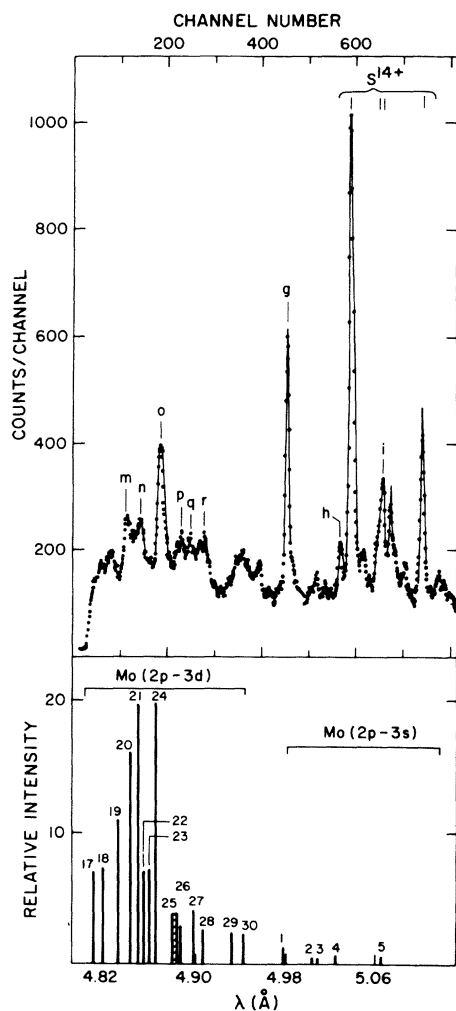


FIG. 6. Comparison of experimental and theoretical spectra in the region of Mo ($2p-3d$) (Table IV) and ($2p-3s$) (Table V) transitions. Experimental spectrum is an addition of 20 shots at $\bar{N}_e = 1.7 \times 10^{14} \text{ cm}^{-3}$ and $T_e \approx 1.6 \text{ keV}$.

$n=2$ to $n=1$ He-like spectrum of sulfur, which here provided us with the wavelength calibration.^{21,22} This part of the Mo line-emission spectrum is always dominated by the peak at 4.982 Å. This peak is identified with the calculated line 1 (i.e., a $2p_{1/2}-3s$ transition in Mo^{32+}) as shown in Table V. Except for the two peaks clearly observed at 5.155 and 5.163 Å most of the weaker features can also be correlated with calculated $2p-3s$ transitions. The peaks at 5.207 and 5.217 Å can be accounted for as $2p_{3/2}-3s_{1/2}$ transitions in Mo^{32+} , the latter being of the magnetic quadrupole type. These two lines always appear together in our spectra but are observed with varying relative intensities from one discharge to another.

Having observed Mo^{32+} lines, one would expect

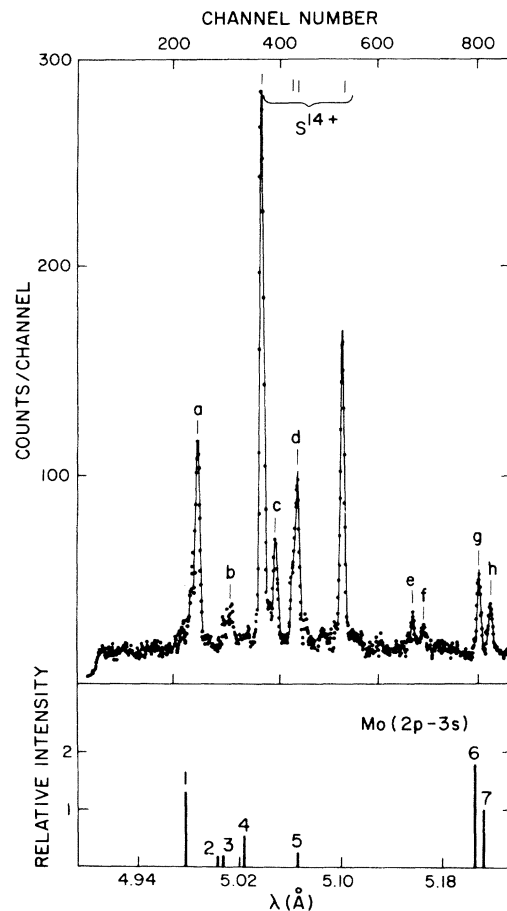


FIG. 7. Comparison of experimental and theoretical spectra in the region of Mo $2p-3s$ transitions. The observed peaks have been keyed with letters and the theoretical predicted ones with numbers referred to in Table V. Experimental spectrum is an addition of five shots at $\bar{N}_e = 2.3 \times 10^{14} \text{ cm}^{-3}$ and $T_e \approx 1.4 \text{ keV}$.

manifestations also from Mo^{31+} and Mo^{30+} just as for the $2p-3d$ transitions. Peaks at 5.063 and 5.065 Å may contain some contributions from predicted $2p_{1/2}-3s$ transitions in Mo^{30+} in this wavelength region, whereas the corresponding transition in Mo^{31+} predicted at 5.024 Å is very weak in our spectra and generally not detectable.

A spectrum bridging the wavelength regions of $2p-3s$ and $2p-3d$ transitions is shown in Fig. 6. The keys in the figure refer to Tables IV and V for the $2p-3d$ and $2p-3s$ transitions, respectively. All the major peaks have been identified as discussed before, and this spectrum essentially shows the relative intensities of $2p-3s$ and $2p-3d$ transitions. Other rather weak and broad features appear in the region of $\lambda \approx 4.93-4.94 \text{ Å}$ which could be ascribed to transitions from the lower ionization stages $\text{Mo}^{28+}-\text{Mo}^{30+}$ (see Table IV).

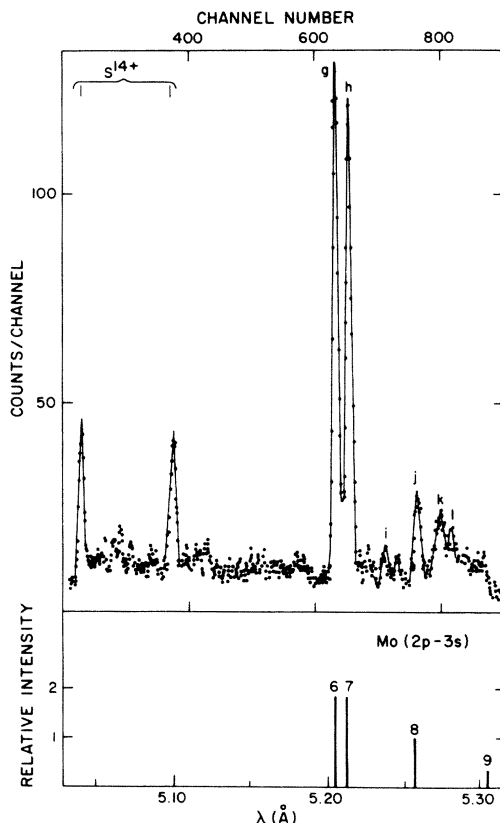


FIG. 8. Comparison of experimental and theoretical spectra in the region of Mo $2p$ - $3s$ transitions. Experimental spectrum is an addition of three shots at $\bar{N}_e = 2.0 \times 10^{14} \text{ cm}^{-3}$ and $T_e \approx 1.4 \text{ keV}$.

A special effort was made to search for the predicted $2p$ - $3s$ transitions in Mo^{30+} and Mo^{31+} in the region of $\lambda > 5.22 \text{ \AA}$, which is at the end of the spectrometer bandwidth. Figure 8 shows the result for this wavelength region with a clear peak at 5.259 \AA which is very suggestive of the predicted Mo^{31+} $2p_{3/2}$ - $2s_{1/2}$ line at 5.256 \AA . Another peak appears at 5.274 \AA and beyond this peak there is a broad structure extending to the experimental cutoff at about 5.31 \AA . A $2p_{3/2}$ - $3s_{1/2}$ line in Mo^{30+} is predicted at 5.304 \AA , but it is highly questionable that this weak line is observed. Thus this broad feature and the $5.274\text{-}\text{\AA}$ peak in the measured spectrum have not been theoretically accounted for which is true also for the peaks (c, e, and f) at 5.049 , 5.155 , and 5.163 \AA (Fig. 7). Of the predicted principal $2p_{1/2}$ - $3s_{1/2}$ and $2p_{3/2}$ - $3s_{1/2}$ transitions in Mo^{32+} , Mo^{31+} , and Mo^{30+} we have not been able to localize experimental counterparts to the transitions $2p_{1/2}$ - $3s_{1/2}$ in Mo^{31+} and $2p_{3/2}$ - $3s_{1/2}$ in Mo^{30+} .

C. $2s$ - $3p$ transitions

The observed spectrum in Fig. 4 covering $\lambda = 4.3\text{--}4.7 \text{ \AA}$ shows two distinct groups of line contributions. The lines in the region $\lambda > 4.60 \text{ \AA}$ have already been identified as $2p$ - $3d$ transitions in molybdenum. The region $4.40\text{--}4.55 \text{ \AA}$ contains the well-known lines of the He-like spectrum of Cl^{15+} .^{11,22} The remaining peaks seen in this region are attributed to $2s$ - $3p$ transitions in molybdenum. The peak labeled *a* can be identified with the predicted $2s_{1/2}$ - $3p_{3/2}$ transition in Mo^{32+} at 4.412 \AA , while the $2s_{1/2}$ - $3p_{1/2}$ transition seems to have no obvious experimental counterpart or is hidden under the $1s$ - $2p$ lines from Cl^{15+} . Peaks *b* and *c* can be accounted for by $2s$ - $3p$ transitions in Mo^{31+} , and there may also be some weak traces in the observed spectrum of Fig. 4 of the predicted lines 3 and 5, where the latter would indicate the presence of Mo^{30+} . However, the Mo^{31+} and Mo^{30+} lines have observed intensities relative to Mo^{32+} that are much weaker than predicted. We also note that all $2s$ - $3p$ transitions are observed to be quite weak relative to the $2p$ - $3d$ transitions which always dominate our emission spectra for molybdenum.

V. DISCUSSION

We have shown that calculated $2s$ - $3p$, $2p$ - $3s$, and $2p$ - $3d$ transitions in molybdenum of charge states $28+ \text{--} 32+$ can account for most of the observed emission spectrum in the λ range $4.3\text{--}5.3 \text{ \AA}$. Some of the many small peaks observed, sometimes appearing as quasicontinuum regions, could indicate emission from other, lower ionization states of molybdenum. Another possibility is that the dominant ionization states are $28+ \text{--} 32+$ but with contributions from dielectronic-recombination excitation besides the collisional excitations determining the principal transitions. We have thus calculated the $2p$ - $3d$ line spectra for $\text{Mo}^{28+}\text{--}\text{Mo}^{32+}$ to obtain an estimate for the effect of contributions of doubly excited states reached through dielectric recombination which can be considered as the satellite-line spectrum. Table VI gives a comparison of contributions from dielectronic recombination to the $2p$ - $3d$ transitions, where we consider two cases of occupancy for electrons in $\text{Mo}^{29+}\text{--}\text{Mo}^{31+}$. In the first case the spectator is limited to occupying $n=3$ states (column B in Table VI) and in the other it can occupy either $n=3$ or 4 (column C). These results are compared with the spectrum due to collisional excitation only and hence singly excited upper states (column A). We thus note that there is a significant contribution to the spectrum from dielectronic recombination, especially for $n=3$ spectators. Al-

TABLE VI. Comparison of contributions ($T_e = 1.2$ keV) for dielectronic-recombination satellites to the total line strength for Mo $2p-3d$ transitions for three cases: (A) collisional excitation only, $\text{Mo}^{28+}-\text{Mo}^{32+}$; (B) including $\text{Mo}^{29+}-\text{Mo}^{31+}$ satellites belonging to $n=3$ spectator electrons; and (C) including $\text{Mo}^{29+}-\text{Mo}^{31+}$ satellites belonging to $n=3$ and 4 spectator electrons.

Figure keys (Fig. 5)	λ_{theor} (Å)	A	B	C
1	4.625	22	25	25
2	4.628	6.7	6.7	6.7
	4.633			2.6
3	4.643		1.8	2.4
4	4.648		1.8	2.2
5	4.659	10.4	17	19
6	4.665	12.2	13	14
7	4.674—4.675	18.7	24	25
8	4.689			
9	4.693	1.2	6.8	9.3
10	4.699	3.3	5.5	6.7
11	4.705			
12	4.708	3.5	5.0	6.5
	4.715			5.4
13	4.723		1.0	1.0
14	4.726	4.3	4.3	4.3
15	4.740—4.751	2.5	3	5
16	4.802	24	24	24
17	4.813	7.1	7.1	11
18	4.820	7.2	7.2	7.2
19	4.833	4.2	11	13
20	4.842	10.7	16	22
21	4.840	14	20	20
22	4.855			
23	4.858	3.4	7	7
24	4.866	10.8	20	22
	4.874			6.1
25	4.880—4.883	2.4	3.8	4.2
26	4.887	2.8	2.8	4.5
	4.893			8.5
27	4.899	3.1	4.2	5.4
28	4.905	1.6	2.5	7
	4.910			5.3
29	4.931	2.3	2.3	2.3
30	4.940	2.1	2.1	2.1

though the main spectral features observed seem to emanate from radiative transitions from the collisionally excited states there are other complex spectral features, particularly on the long-wavelength side of the Mo^{32+} line at 4.804 Å. The relative intensities of these spectral features are found to vary considerably between different discharges, while those of the identified resonance transitions remain largely unchanged relative to each other. An example of this can be found in Fig. 9 which shows spectra from three consecutive single

discharges. These intensity variations could be attributed to temperature changes which would show up most strongly in the relative intensities of the satellite lines.

In this context it is also interesting to consider the relative importance of the dielectronic-recombination radiation as part of the total x-ray emission from the molybdenum ions in this energy range. As an illustration, we calculated the radiative power from dielectronic recombination relative to that due to collisional excitation for $\Delta n = 1$ transi-

TABLE VII. Comparison of the calculated radiative power from states excited by electron collisions and dielectronic recombination for $\Delta n = 1$ transitions in the wavelength region $\lambda = 4.3 - 5.3 \text{ \AA}$ in plasmas of $T_e = 0.8, 1.2,$ and 2.0 keV .

Mo charge state $2p-3d$ transitions	Spectator nl	Radiated Power (W/cm^3)					
		$T_e = 0.8 \text{ (keV)}$		$T_e = 1.2 \text{ keV}$		$T_e = 2.0 \text{ keV}$	
		Collision	Dielectronic recombination	Collision	Dielectronic recombination	Collision	Dielectronic recombination
28 +		0.0185		0.0452		0.0876	
	29 +		0.100		0.083		0.054
	29 +		0.031		0.035		0.030
29 +	3p, 3d						
	4s, 4p, 4d, 4f	0.0301		0.0737		0.144	
	30 +		0.183		0.149		0.096
	30 +		0.045		0.050		0.041
30 +	3s, 3p, 3d						
	4s, 4p, 4d, 4f	0.0459		0.113		0.222	
	31 +		0.120		0.096		0.060
	31 +		0.032		0.035		0.029
31 +	3s, 3p, 3d	0.0572		0.142		0.278	
32 +	4s, 4p, 4d, 4f	0.0420		0.102		0.196	
$\Sigma(28+ - 32+)$		0.194	0.511	0.476	0.448	0.928	0.310
$2p-3d$		0.007		0.016		0.029	
$\Sigma(28+ - 32+)$		0.026		0.069		0.140	
$2p-3s$							
$\Sigma(28+ - 32+)$							
$2s-3p$							

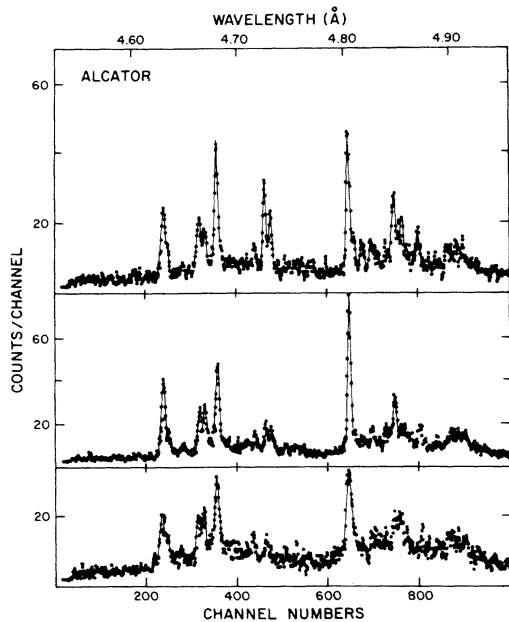


FIG. 9. Three consecutive plasma shots with similar parameters $\bar{N}_e = 2.9 \times 10^{14} \text{ cm}^{-3}$ and $T_e \approx 1.4 \text{ keV}$.

tions in the wavelength region of our study, $\lambda = 4.3\text{--}5.3 \text{ \AA}$. We assumed the electron density to be $\bar{N}_e = 10^{14} \text{ cm}^{-3}$ with $N_{\text{ion}} = 10^{12} \text{ cm}^{-3}$. The ionization abundance distribution for the molybdenum charge states (Mo^{28+} – Mo^{32+}) we take to be independent of temperature and as given earlier, i.e., the fractions were 0.08, 0.13, 0.20, 0.25, and 0.17, respectively. The results are shown in Table VII for three different temperatures ($T_e = 0.8, 1.2,$ and 2.0 keV), distinguishing between contributions from the states due to collisional excitation and dielectronic recombination. It is found that influence of dielectronic recombination is appreciable for the $\Delta n = 1$ transitions at these temperatures and must be considered in determining the energy balance of the plasma.

With regard to the information of the x-ray line spectrum of molybdenum from previous experiments we note the studies of laser-induced plasmas.⁸ These spectra, which also cover the wavelength range $4.4\text{--}5.3 \text{ \AA}$, are similar to ours in that the same transitions are found to dominate in both cases. Of the 15 Mo lines reported from the laser work there are matching counterparts found in our spectra to all but two of the lines. The lines at 4.461 and 4.689 \AA corresponding to $\text{Mo}^{32+} 2s\text{-}3p$ and $\text{Mo}^{31+} 2p\text{-}3d$ transitions are missing in our spectra or too weak to be detected; the latter cannot be ruled out since the relative line intensities are not always the same in spectra of the laser and tokamak plasmas. On the other hand, our spectra show many lines not previ-

ously reported in either the laser studies or in exploding-wire experiments.¹⁶ Of these lines we mention the magnetic quadrupole transition at 5.217 \AA for which a relationship to plasma conditions can be identified. The fact that this line is missing in other than the low-density tokamak plasmas can be seen as a manifestation of collisional depletion of the metastable upper state for plasmas of higher densities such as those produced by laser irradiation.

VI. CONCLUSIONS

We have measured characteristic x-ray emission of molybdenum in the wavelength range $\lambda = 4.4\text{--}5.3 \text{ \AA}$ and interpreted the observed line spectrum with the help of computed Hartree-Fock spectra which are also presented. The strongest transitions are found to be $2p\text{-}3d$ in Mo^{32+} , Mo^{31+} , and Mo^{30+} along with $2p\text{-}3s$ and $2s\text{-}3p$ transitions. The wavelength agreement between experiment and theory is typically 5 m\AA or better while the calculated spin-orbit splittings tend to be systematically too large relative to observation. The latter observations could be further investigated by comparison with fully relativistic Dirac-Fock calculations where the spin-orbit interaction is a natural part of the theory. With regard to relative line intensities we do observe quite large differences between measured and computed spectra which in part can be referred to the rather crude excitation rates employed for calculating line intensities. It still seems that additional population mechanisms might be needed since differences between experiment and theory tend to occur also for the principal transitions of same ion charge states for which one would expect the line intensity to be determined by the ground-state excitation rate and hence simply by the oscillator strengths. This experiment also suggests that the ratio of ionization to dielectronic-recombination rates for neonlike molybdenum and possibly other isoelectronic ions is larger than expected based on the observation of Mo^{32+} at temperatures of $1.0\text{--}1.5 \text{ keV}$ compared to the predicted relative peak abundance of Mo^{32+} at a factor of 2 higher temperatures.

ACKNOWLEDGMENTS

The collaboration with the Alcator group is gratefully acknowledged. This work was supported by the United States Department of Energy.

- ¹A. H. Gabriel, *Mon. Not. R. Astron. Soc.* **160**, 99 (1972).
- ²D. E. Post *et al.*, *At. Data Nucl. Data Tables* **20**, 397 (1977).
- ³A. L. Merts, R. D. Cowan, and N. H. Magee, Jr., Los Alamos National Laboratory Report No. LA-6220-MS (unpublished).
- ⁴C. Breton, C. DeMichelis, M. Finkenthal, and M. Mattioli, Association Euratom Commissariat à L'Energie Atomique Report No. EUR-CEA-FC-948 (unpublished); C. Breton *et al.*, Report No. EUR-CEA-FC-1159 [*J. Phys. B* (in press)]; *Phys. Rev. Lett.* **41**, 110 (1978).
- ⁵C. Breton, C. DeMichelis, and M. Mattioli, *J. Quant. Spectrosc. Radiat. Transfer* **19**, 367 (1978).
- ⁶P. G. Burkhalter, J. Reader, and R. D. Cowan, *J. Opt. Soc. Am.* **67**, 1521 (1977); **70**, 912 (1980).
- ⁷U. Feldman, *Phys. Scr.* **24**, 680 (1981).
- ⁸H. Gordon, M. G. Hobby, N. J. Peacock, and R. D. Cowan, *J. Phys. B* **12**, 881 (1979).
- ⁹M. Klapisch, *Phys. Scr.* (in press).
- ¹⁰B. Blackwell *et al.*, in *Plasma Physics and Controlled Nuclear Fusion Research (Proceedings of the Ninth International Conference, Baltimore, 1982)* (IAEA, Vienna, 1983).
- ¹¹E. Källne, J. Källne, and J. E. Rice, *Phys. Rev. Lett.* **49**, 330 (1982).
- ¹²E. Källne and J. Källne, *Phys. Scr.* (in press).
- ¹³E. Källne, J. Källne, and A. J. Pradhan, *Phys. Rev. A* **27**, 1476 (1983).
- ¹⁴E. Källne and J. Källne, *X-Ray and Atomic Inner Shell Physics—1982, (International Conference, University of Oregon)* AIP Conf. Proc. No. 94, edited by B. Crasemann (AIP, New York, 1978), p. 463.
- ¹⁵E. V. Aglitskii *et al.*, *Kvant. Elektron. (Moscow)* **1**, 2067 (1974) [*Sov. J. Quantum Electron.* **4**, 1152 (1975)]; **1**, 908 (1974) [**4**, 500 (1974)].
- ¹⁶P. G. Burkhalter, R. Schneider, C. M. Dozier, and R. D. Cowan, *Phys. Rev. A* **18**, 718 (1978).
- ¹⁷R. D. Cowan, *The Theory of Atomic Structure and Spectra* (University of California Press, Berkeley, 1981).
- ¹⁸R. D. Cowan and D. C. Griffin, *J. Opt. Soc. Am.* **66**, 1010 (1976); **58**, 808 (1968).
- ¹⁹R. D. Cowan, *Phys. Scr.* (in press).
- ²⁰H. Van Regemorter, *Astrophys. J.* **136**, 906 (1962).
- ²¹L. A. Vainshtein and U. I. Safronova, *At. Data Nucl. Data Tables* **21**, 49 (1978).
- ²²U. I. Safronova, *Phys. Scr.* **23**, 241 (1981).